arXiv:1607.00032v2 [astro-ph.CO] 25 Nov 2016

A Combined View of Sterile-Neutrino Constraints from CMB and Neutrino Oscillation Measurements

Sarah Bridle, Jack Elvin-Poole, Justin Evans, Susana Fernandez, Pawel Guzowski, Stefan Söldner-Rembold

The University of Manchester, School of Physics and Astronomy, Manchester, M13 9PL, United Kingdom

Abstract

We perform a comparative analysis of constraints on sterile neutrinos from the Planck experiment and from current and future neutrino oscillation experiments (MINOS, IceCube, SBN). For the first time, we express joint constraints on $N_{\rm eff}$ and $m_{\rm eff}^{\rm sterile}$ from the CMB in the Δm^2, $\sin^2 2\theta$ parameter space used by oscillation experiments. We also show constraints from oscillation experiments in the $N_{\rm eff}$, $m_{\rm eff}^{\rm sterile}$ cosmology parameter space. In a model with a single sterile neutrino species and using standard assumptions, we find that the Planck 2015 data and the oscillation experiments measuring muon-neutrino (ν_μ) disappearance have similar sensitivity.

Keywords: Sterile Neutrinos, Cosmology, Oscillation Experiments

1. Introduction

The search for low-mass sterile neutrinos is motivated by several experimental anomalies that are not consistent with the three-flavour paradigm. Sterile neutrinos would change the oscillation probabilities observed by detecting neutrinos from accelerators, nuclear reactors, or produced in the atmosphere. On a cosmological scale, they would modify the power spectrum of the Cosmic Microwave Background (CMB) (Fig. 1).

Both types of measurement put severe constraints on the existence of extra neutrino flavours, but they are evaluated in terms of different parameter sets. The CMB measurements constrain the effective number of additional neutrino species, $\Delta N_{\rm eff}$ (above the Standard Model (SM) prediction of $N_{\rm eff} = 3.046$), and the effective sterile neutrino mass $m_{\rm eff}^{\rm sterile}$. Oscillation experiments

parameterize their constraints in terms of mass-squared differences, Δm^2_{ij}, between the mass eigenstates, and the mixing angles $\theta_{\alpha\beta}$ between mass and flavour eigenstates. Here, we use the calculation of [1] and show the Planck CMB cosmology constraints in the same parameter space as used for ν_μ disappearance measurements.

Several experimental anomalies related to the appearance and disappearance of ν_e could be explained by light sterile neutrinos with a mass-squared difference relative to the active states of $\Delta m^2 \approx 1\,\mathrm{eV}^2$ [2, 3, 4]. The LSND Collaboration observes an excess of $\bar{\nu}_e$ appearance in a $\bar{\nu}_\mu$ beam [5], and MiniBooNE measures an excess of both ν_e [6] and $\bar{\nu}_e$ appearance [7, 8]. Reactor experiments observe a deficit of $\approx 6\%$ in the $\bar{\nu}_e$ flux compared to expectations [9]. Furthermore, Gallium experiments observe a smaller $\nu_e + {}^{71}\mathrm{Ga} \rightarrow {}^{71}\mathrm{Ge} + e^-$ event rate than expected from ${}^{51}\mathrm{Cr}$ and ${}^{37}\mathrm{Ar}$ sources [10]. The Daya Bay Reactor experiment has searched for $\bar{\nu}_e$ disappearance setting limits on the mixing angle $\sin^2\theta_{14}$ in the low Δm^2 region $0.0002 < \Delta m^2_{41} < 0.2\,\mathrm{eV}^2$ [11]. These results have been combined with ν_μ disappearances searches by MINOS [12] to obtain stringent constraints on the product $\sin^2 2\theta_{14} \sin^2\theta_{24}$ [13]. For this analysis, we focus on recent ν_μ disappearance results, where no anomalies have been found, and assume that $\sin^2\theta_{14} = \sin^2\theta_{34} = 0$ in order to be consistent with the assumptions that were used for deriving these limits.

Several studies have combined oscillation and cosmological data to constrain sterile neutrinos. Several [14, 15, 16, 17, 18] use the posterior probability distribution on Δm^2 from short-baseline anomalies as a prior in the cosmological analysis. Here, we convert the full CMB cosmology constraints into the oscillation parameterisation and vise versa, focusing on recent ν_μ disappearance results. This conversion has also been studied in [19, 20]. Our analysis differs in several ways: (i) unlike [19] we use the 2D combined constraints on ΔN_{eff} and $m_{\mathrm{eff}}^{\mathrm{sterile}}$ in the cosmological analysis, rather than converting 1D constraint values in each parameter individually; (ii) we use the latest CMB data from Planck, updating from the WMAP 5-year data used in [20]; (iii) we solve the full quantum kinetic equations, rather than using the averaged momentum approximation [21] used in [19, 20]; (iv) we also consider the impact of non-zero lepton asymmetry, L, and a different sterile mass mechanism. The lepton asymmetry is defined as $L = (n_f - n_{\bar{f}})N_f/N_\gamma$, where n_f and $n_{\bar{f}}$ are the number densities of fermions and anti-fermions, respectively, and N_f and N_γ are the numbers of fermions and photons.

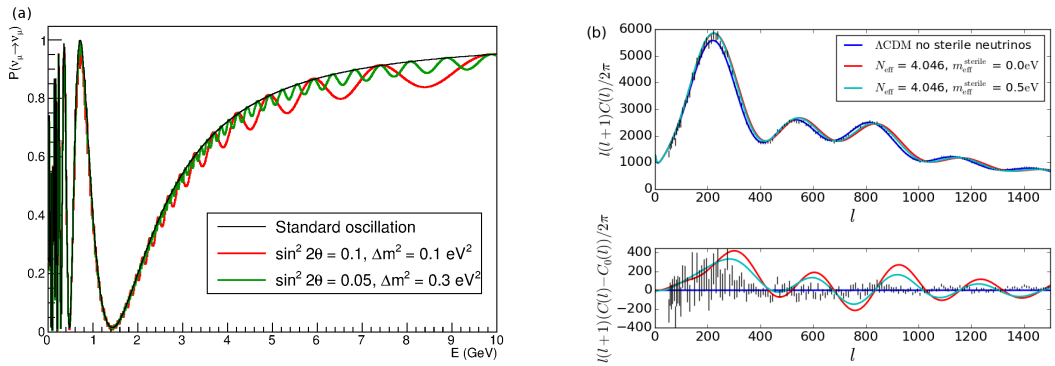

Figure 1: (a) The ν_μ survival probability after 735 km as a function of neutrino energy, for different oscillation parameter values. (b) The CMB temperature power spectrum for different values of the effective number of neutrino species and effective sterile mass, fixing the cold dark matter energy density. The ΛCDM case uses the SM value $N_{\rm eff} = 3.046$ and an active neutrino mass sum $\sum m_\nu = 0.06\,$eV. All other cosmological parameters are set to the best-fit values from the Planck 2015 data shown by error bars [32]. The power spectra are generated using the CAMB module [33] in CosmoSIS [34].

2. Data sets

2.1. Cosmological Data sets

Observations of the CMB radiation are the most powerful probe of cosmology, giving a snapshot of the Universe around 300,000 years after the Big Bang. The angular intensity fluctuations are sourced by temperature fluctuations in the plasma, which in turn depend on the constituents of the Universe, including sterile neutrinos. Cosmology results are most sensitive to the sum of all neutrino masses, rather than the relative masses of the active and sterile neutrinos. The Planck Satellite currently provides the definitive measurement of the CMB temperature anisotropies [22]. The Planck data have been used to constrain the sum of the active neutrino masses yielding $\sum m_\nu < 0.68\,$eV from CMB temperature data alone [23]. The information from the CMB can also be combined with that from other cosmological observations for even tighter constraints [24, 25, 26, 27, 28, 29, 30, 31]. Here, we use the Planck temperature power spectrum and low multipole polarisation data alone.

To constrain sterile neutrinos, two parameters are added to the baseline Planck analysis: the effective sterile mass, $m_{\rm eff}^{\rm sterile} = (94.1\,\Omega_{\rm sterile}h^2)\,$eV, and the effective number of additional neutrino species, $\Delta N_{\rm eff} = N_{\rm eff} - 3.046$.

The cosmological model used is $\Lambda\mathrm{CDM} + m_{\mathrm{eff}}^{\mathrm{sterile}} + \Delta N_{\mathrm{eff}}$. Additional cosmological parameters and their degeneracies with neutrino parameters are not considered here.

Figure 1 (b) shows the power spectrum of the CMB temperature fluctuations. We observe that increasing the effective number of neutrino species, while fixing $m_{\mathrm{eff}}^{\mathrm{sterile}} = 0$, shifts the peak structure to higher multipoles, l, due to a change in the matter-radiation equality redshift, z_{eq}. There is also an increase in the integrated Sachs-Wolfe effect at low l [35]. A non-zero $m_{\mathrm{eff}}^{\mathrm{sterile}}$ further changes z_{eq} adding to the shift of the peak locations [36, 2, 35, 37].

The effective mass, $m_{\mathrm{eff}}^{\mathrm{sterile}}$, can be related to the mass of the sterile neutrino, $m_{\mathrm{sterile}} = m_4$, in two ways. The first is to assume a thermal distribution with an arbitrary temperature T_s. The quantity ΔN_{eff} is then a measure of the thermalisation of the sterile neutrinos, $\Delta N_{\mathrm{eff}} = (T_s/T_\nu)^4$, yielding,

$$m_{\mathrm{eff}}^{\mathrm{sterile}} = \left(\frac{T_s}{T_\nu}\right)^3 m_4^{\mathrm{thermal}} = (\Delta N_{\mathrm{eff}})^{3/4} m_4^{\mathrm{thermal}} \,. \tag{1}$$

The second model assumes the extra eigenstate is distributed proportionally to the active state by a scaling factor, χ_s, here equal to ΔN_{eff},

$$m_{\mathrm{eff}}^{\mathrm{sterile}} = \chi_s m_4^{\mathrm{DW}} = \Delta N_{\mathrm{eff}} m_4^{\mathrm{DW}} \,. \tag{2}$$

This is known as the Dodelson-Widrow (DW) mechanism [38]. We use the thermal distribution as our fiducial interpretation and show that our conclusions are robust to this choice.

The Planck analysis assumes the normal mass ordering of the active neutrinos with the minimum masses allowed by oscillation experiments, $m_1 = 0\,\mathrm{eV}$, $m_2 \approx 0\,\mathrm{eV}$, and $m_3 = 0.06\,\mathrm{eV}$. Any excess mass is considered to be from a single additional state, which implies that $\Delta m_{41}^2 \approx m_4^2$. We use these assumptions throughout our analysis. Assuming inverted mass ordering or allowing $m_1 > 0$ would strengthen the Planck constraints on sterile neutrinos. These assumptions allow us to directly compare to the oscillation data. The Planck 95% Confidence Level (CL) contour is shown in Fig. 2 (b, d) for a prior of $m_4^{\mathrm{thermal}} < 10$ eV [23].

2.2. Oscillation Data sets

The MINOS experiment [39] reconstructs interactions from a ν_μ beam created in an accelerator at Fermilab in a near detector (ND), located about 1 km from the source, and a far detector (FD) at 735 km. A sterile neutrino

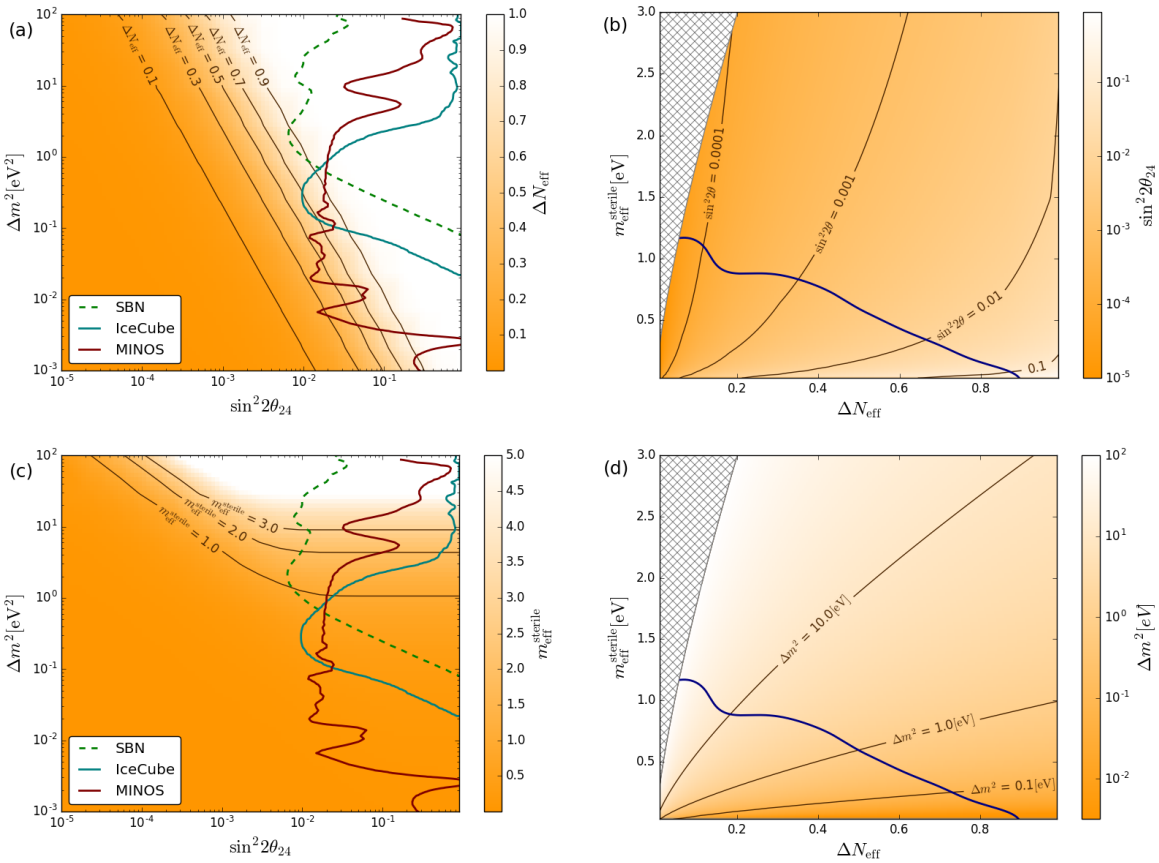

Figure 2: (a, c) Cosmological parameters $\Delta N_{\rm eff}$ and $m_{\rm eff}^{\rm sterile}$ calculated in the oscillation space Δm^2, $\sin^2 2\theta_{24}$ using LASAGNA. We use the thermal sterile neutrino mass (Eq. 1) and $L = 0$. Also shown are the constraints from the experiments native to this space, MINOS and IceCube, and the SBN sensitivity. The region to the right of the contours is ruled out at the 95% CL. (b, d) Δm^2, $\sin^2 2\theta$ in the cosmological space, $m_{\rm eff}^{\rm sterile}$, $\Delta N_{\rm eff}$. The region above the blue line is excluded by the Planck temperature and low-l polarization data at 95% CL. A prior of $m_4^{\rm thermal} < 10\,{\rm eV}$ has been applied as in [23]. The hatched area corresponds to $m_4^{\rm thermal} > 10\,{\rm eV}$ where $\Delta N_{\rm eff}$ was not calculated.

will reduce the ν_μ survival probability through its mixing with the active neutrinos (Fig. 1 (a)). In most analyses, the ND serves as a reference point that defines the un-oscillated beam spectrum. However, for mass differences above $\Delta m^2 \approx 1\,\mathrm{eV}^2$, oscillations occur rapidly and can already lead to a depletion of the neutrino flux at the ND. MINOS has therefore performed an innovative analysis exploiting the ratio of the neutrino energy spectra measured in the FD to those in the ND using both charged-current (CC) ν_μ and neutral-current (NC) neutrino interactions [40, 12]. Limits on sterile-neutrino parameters are obtained by performing a χ^2 fit of the far-over-near ratio for both CC and NC data samples.

We use the χ^2 surface given in [40], which includes the data published in [12] and incorporates the statistical uncertainties, a full covariance matrix of the experimental systematic uncertainties, and a weak constraint on Δm^2_{32}, which the data can then itself constrain. All other three-flavour oscillation parameters are fixed in the MINOS fit. We assume that all uncertainties follow a Gaussian distribution, and derive confidence levels using Gaussian χ^2 p-values. The 95% CL contour derived from the MINOS χ^2 distribution is shown in Fig. 2 (a, c).

The IceCube detector [41] comprises 5160 optical modules instrumenting $\sim$1 km^3 of ice at the South Pole. Neutrinos are detected using Cherenkov radiation emitted by charged particles produced in CC interactions. This is used to measure the disappearance of atmospheric muon neutrinos (ν_μ and $\bar{\nu}_\mu$) that have traversed the Earth. Sterile neutrinos are expected to modify the energy-dependent zenith-angle distribution of the ν_μ and $\bar{\nu}_\mu$ through resonant matter-enhanced oscillations caused by the MSW effect [42, 43]. IceCube has searched for sterile neutrinos by studying the 2D distribution of the reconstructed neutrino energy and zenith angle [44, 45].

The IceCube likelihood distribution utilizes both shape and rate information, including systematic and statistical uncertainties. The distributions shown in Fig. 2 (a, c) are taken from [45]. The IceCube Collaboration also assumes $\theta_{34} = 0$ in its analysis. It shows that this assumption leads to a more conservative limit and that non-zero values of θ_{14} have little effect on the results [44].

The Short Baseline Neutrino (SBN) programme [46] at Fermilab will study the LSND [5] and MiniBooNE [6, 7, 8] anomalies. It comprises three liquid-argon time projection chambers at different baselines in a ν_μ beam: the already-running MicroBooNE detector, and the SBND and ICARUS detectors that are due to start data-taking in 2018. The programme will primarily

search for ν_e appearance, but can also study the disappearance of ν_μ.

We use GLOBES [47] to estimate the SBN sensitivity in the ν_μ disappearance channel. The GENIE Monte Carlo (MC) generator [48] is used to calculate the ν_μ CC interaction cross section on argon. We develop a toy MC model to calculate the geometric acceptance, using the GENIE output of muon momentum and direction, muon range tables [49], and interaction vertices distributed uniformly inside the active dimensions of the detectors. Acceptances are calculated for fully-contained muons, or for exiting muons with a track length of at least 1 m inside the detector. Energies of contained muons are smeared by a 2% absolute resolution, while for exiting muons the resolution is assumed to be $10\%/\sqrt{E[\mathrm{GeV}]}$. Hadronic energy is smeared by $20\%/\sqrt{E[\mathrm{GeV}]}$. We apply an overall selection efficiency of 80%.

We combine the beam fluxes from Fig. 3 of [46] with the modeled efficiencies and energy-smearing matrices to provide inputs to GLOBES, which is used to calculate the χ^2 surface as a function of the mixing angle θ_{24} and mass-squared difference Δm^2_{41}. We always set $\theta_{14} = \theta_{34} = 0$. Only the ν_μ disappearance channel is used to make a direct comparison with the MINOS and IceCube measurements in Figs. 2 (a, c).

3. Thermalisation of sterile neutrinos

To relate the cosmological parameterization ($m_{\mathrm{eff}}^{\mathrm{sterile}}$, ΔN_{eff}) to the oscillation parameterization (Δm^2_{ij}, $\theta_{\alpha\beta}$), we solve the full quantum kinetic equations that govern the sterile neutrino thermalization [1]. We use LASAGNA [50] to solve these equations in the simplified scenario with one active and one sterile neutrino flavour as described in [51, 52]. This scenario contains a single mixing angle, θ, and the flavour states are

$$\nu_a = \cos\theta\nu_1 - \sin\theta\nu_2\,, \tag{3}$$

$$\nu_s = \sin\theta\nu_1 + \cos\theta\nu_2\,, \tag{4}$$

where $\nu_{1,2}$ are the mass eigenstates, and $\nu_{a,s}$ the active and sterile flavour eigenstates, respectively.

The LASAGNA input parameters are the mass splitting, Δm^2, between the two mass states, the mixing angle, θ, the lepton asymmetry, L, and the range in temperature, T, over which to evolve the kinetic equations. LASAGNA produces a grid in the parameter $x = p/T$, where p is the neutrino momentum, upon which the factor

$$P_s^+ = (P_0 + \bar{P}_0) + (P_z + \bar{P}_z) \tag{5}$$

is calculated. Here, P_0 and P_z are the first and last components of the neutrino Bloch vector, (P_0, P_x, P_y, P_z). The factor P_0 corresponds to the number density of the mixed state, and P_z is related to the probability that a neutrino is in the sterile or active state, $\mathrm{Prob}(\nu_s) = (1 - P_z)/2$, and $\mathrm{Prob}(\nu_a) = (1 + P_z)/2$. The factors $\bar{P}_0$ and $\bar{P}_z$ are the corresponding anti-neutrino values. We use P_s^+ to calculate

$$\Delta N_{\mathrm{eff}} = \frac{\int dx\, x^3 f_0 P_s^+}{4 \int dx\, x^3 f_0} \tag{6}$$

with the Fermi-Dirac distribution function, $f_0 = 1/(1 + e^x)$. This is valid if the active states are in thermal equilibrium. More details on LASAGNA are given in [1, 50] and on the quantum kinetic equations in [51, 52].

For our fiducial analysis, we run LASAGNA with $L = 0$ in a temperature range $1 < T < 40\,\mathrm{MeV}$, calculating ΔN_{eff} on the 2D grid of Δm^2, $\sin^2 2\theta$ values shown in Fig. 2 (a). We convert positions in the cosmology parameter space ($m_{\mathrm{eff}}^{\mathrm{sterile}}$, ΔN_{eff}) into the oscillation space (Δm_{41}^2, $\sin^2 2\theta_{24}$), first by using $\Delta m_{41}^2 = m_4^2$ and Eq. 1 to find Δm_{41}^2, then interpolating $\sin^2 2\theta_{24}$ from the underlying grid in Fig. 2. We assume that the sterile-active mixing is dominated by a single angle θ_{24}.

4. Results

The experimental inputs have been derived using different statistical approaches. For the oscillation experiments a $\Delta\chi^2$ contour is calculated as the difference of the χ^2 of the best-fit hypothesis for the data to the χ^2 at each model point. For the Planck data, a multi-dimensional Markov Chain MC is produced allowing cosmological, nuisance and neutrino parameters (ΔN_{eff}, $m_{\mathrm{eff}}^{\mathrm{sterile}}$) to be varied. The number density of points in this chain is proportional to the likelihood $\mathcal{L}$. We draw this likelihood surface in the (ΔN_{eff}, $m_{\mathrm{eff}}^{\mathrm{sterile}}$) plane and take the χ^2 to be $-2\ln(\mathcal{L})$. The contour describing the 95% CL corresponds to $\chi^2 - \chi^2_{\mathrm{min}} = 5.99$ in the 2D input distributions. In the Planck case, this leads to a dependence on the prior of these parameters. In our analysis the priors are flat in the ranges $0 < \Delta N_{\mathrm{eff}} < 1$, and $0 < m_{\mathrm{eff}}^{\mathrm{sterile}} < 3\,\mathrm{eV}$.

We make several standard assumptions about the cosmological and neutrino models that may impact our conclusions. We assume Λ_{CDM} in the Planck analysis and a single sterile neutrino species, mixing only by one channel, in our conversion between parameter spaces. We also assume that any

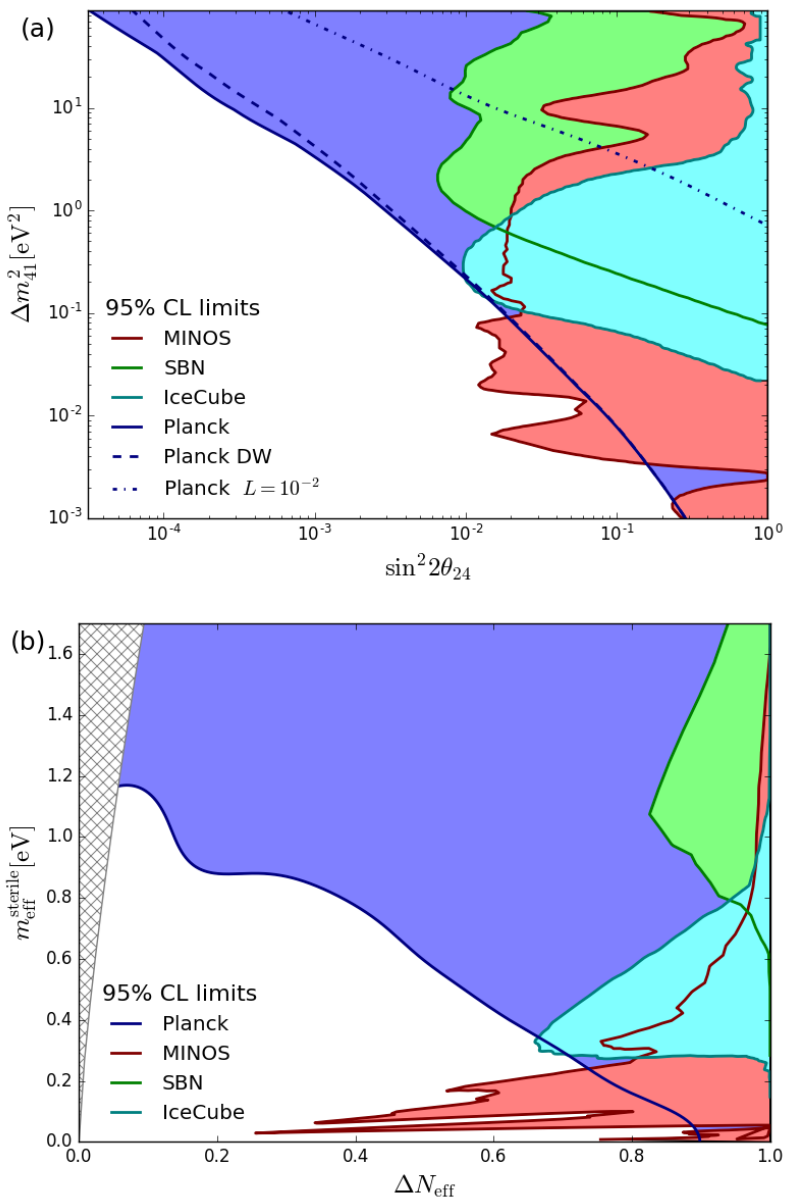

Figure 3: (a) Sterile neutrino exclusion regions at 95% CL from Planck, MINOS, IceCube, and the SBN forecast in the oscillation parameter space. The dashed line is the Planck constraint with m_4 calculated using the Dodelson-Widrow mechanism. The dot-dash line is the Planck constraint using a large lepton-asymmetry, $L = 10^{-2}$. (b) The same contours in the cosmological space, where the difference between the thermal and Dodelson-Widrow scenarios is negligible.

$\Delta N_{\rm eff}$ is caused only by neutrinos and no other light relic particle. Studying the impact of these assumptions is beyond the scope of this paper.

Fig. 3 shows the CMB and oscillation experiment exclusion regions on the same axes in the oscillation and cosmology parameter spaces. The CMB data excludes a similar corner of the parameter space to the oscillation experiments, ruling out large mixing angles and large sterile-neutrino masses within the 3+1 model. This conclusion is unchanged by switching from the thermal mass in Eq. (1) to the Dodelson-Widrow mechanism in Eq. (2).

The condition $\Delta m^2_{41} < 10^{-2.4}$, leads to $m_4 < m_3$, and the active masses can no longer be treated as a single state. Therefore, the Planck contour below this value is too conservative. Ref. [19] discusses cosmological constraints in this Δm^2_{41} range.

The Planck contour at large Δm^2_{41} is dominated by the constraint on $m^{\rm sterile}_{\rm eff}$, and at low Δm^2_{41} by the constraint on $\Delta N_{\rm eff}$, as shown in Figs. 2 (a, c). This is also illustrated in Fig. 3 of [19], which converts 1D upper limits on each of these parameters separately, instead of the 2D likelihood surface. Comparing these results to the averaged-momentum approximation results of [19], we find that solving the full quantum kinetic equations results in qualitatively similar constraints.

In the fiducial analysis, we convert between parameter spaces using the assumption $L = 0$. In this case, the Planck data is more constraining than the oscillation experiments for large mass-squared differences, $\Delta m^2_{41} > 10^{-1}\,{\rm eV}^2$, and less constraining than MINOS in the range $10^{-2} < \Delta m^2_{41} < 10^{-1}\,{\rm eV}^2$. When the lepton asymmetry is large, $L = 10^{-2}$, the oscillations between sterile and active neutrinos are suppressed, giving a lower $\Delta N_{\rm eff}$ for the same oscillation parameters (see Fig. 4 of [1]). This weakens the Planck constraints in the oscillation space such that they are now less constraining than all of the oscillation experiments considered, as shown by the dot-dash line in Fig. 3 (a).

The MINOS experiment is particularly sensitive to the region of low Δm^2_{41} because of its baseline and neutrino energy range. This is the only region where the oscillation data are more constraining than the cosmology data when assuming $L = 0$. In the cosmology space, this corresponds to ruling out a region of large $\Delta N_{\rm eff}$ at low $m^{\rm sterile}_{\rm eff}$.

5. Conclusions

In conclusion, we compare sterile neutrino constraints from oscillation experiments and cosmological constraints. We use the quantum kinetic equations to convert between the standard oscillation parameterization of neutrinos (the mass-squared difference and mixing angle) and the cosmology parameterization (the effective sterile neutrino mass and the effective number of neutrino species). We show the relationship between each of the parameter combinations.

We show the Planck 2015 CMB cosmology constraints in the oscillation parameter space and find that they rule out large values of Δm^2_{41} and mixing angle θ. For the fiducial case, the region of parameter space ruled out by IceCube data is already excluded by the Planck CMB constraints. For the first time, we show that much of the MINOS exclusion region is also ruled out by Planck CMB constraints, although for low Δm^2_{41} MINOS is more constraining. The forecast constraints for the SBN experiments are not expected to add to the information already provided by Planck CMB results with these model assumptions. However, their main sensitivity will be through the ν_e appearance searches not considered here. The MINOS data adds the most information to that provided by Planck CMB measurements because it probes the lowest Δm^2.

The power of the Planck CMB constraint is robust to the choice of effective mass definition used in the cosmology model, giving similar results from the thermal and Dodelson-Widrow mechanisms. However, if we allow the lepton asymmetry to be very large ($L = 10^{-2}$), the Planck exclusion region is significantly reduced.

We also show the oscillation experiment constraints in the cosmology parameter space, where the same effect is observed. In this parameter space the MINOS constraints rule out a larger fraction of the region allowed by the CMB.

Acknowledgements

We are grateful to Thomas Tram (ICG Portsmouth) for help running the LASAGNA code. We thank Joe Zuntz and Richard Battye (Manchester), and Steen Hannestad (Aarhus) for helpful discussions. This work has been supported by the Science and Technology Facilities Council, the Royal Society, and the European Research Council.

References

[1] S. Hannestad, I. Tamborra, T. Tram, Thermalisation of light sterile neutrinos in the early universe, J. Cosmol. Astropart. Phys. 2012 (2012) 025–025.

[2] K. Abazajian, et al., Light Sterile Neutrinos: A White Paper, FERMILAB-PUB-12-881-PPD (2012).

[3] G. H. Collin, et al., Sterile Neutrino Fits to Short Baseline Data, Nucl. Phys. B908 (2016) 354–365.

[4] G. H. Collin, et al., First Constraints on the Complete Neutrino Mixing Matrix with a Sterile Neutrino (2016).

[5] A. Aguilar-Arevalo, et al., Evidence for neutrino oscillations from the observation of anti-neutrino(electron) appearance in a anti-neutrino(muon) beam, Phys. Rev. D64 (2001) 112007.

[6] A. A. Aguilar-Arevalo, et al., A Search for electron neutrino appearance at the $\Delta m^2 \sim 1\text{eV}^2$ scale, Phys. Rev. Lett. 98 (2007) 231801.

[7] A. A. Aguilar-Arevalo, et al., Event Excess in the MiniBooNE Search for $\bar{\nu}_\mu \to \bar{\nu}_e$ Oscillations, Phys. Rev. Lett. 105 (2010) 181801.

[8] A. A. Aguilar-Arevalo, et al., Improved Search for $\bar{\nu}_\mu \to \bar{\nu}_e$ Oscillations in the MiniBooNE Experiment, Phys. Rev. Lett. 110 (2013) 161801.

[9] G. Mention, et al., The Reactor Antineutrino Anomaly, Phys. Rev. D83 (2011) 073006.

[10] C. Giunti, M. Laveder, Statistical Significance of the Gallium Anomaly, Phys. Rev. C83 (2011) 065504.

[11] F. P. An, et al., Improved Search for a Light Sterile Neutrino with the Full Configuration of the Daya Bay Experiment, Phys. Rev. Lett. 117 (2016) 151802.

[12] P. Adamson, et al., A search for sterile neutrinos mixing with muon neutrinos in MINOS, Phys. Rev. Lett. 117 (2016) 151803.

[13] P. Adamson, et al., Limits on Active to Sterile Neutrino Oscillations from Disappearance Searches in the MINOS, Daya Bay, and Bugey-3 Experiments, Phys. Rev. Lett. (2016) 151801.

[14] M. Archidiacono, et al., Testing 3+1 and 3+2 neutrino mass models with cosmology and short baseline experiments, Phys. Rev. D 86 (2012) 065028.

[15] M. Archidiacono, et al., Sterile Neutrinos: Cosmology vs Short-BaseLine Experiments, Phys. Rev. D 87 (2013) 125034.

[16] S. Gariazzo, C. Giunti, M. Laveder, Light Sterile Neutrinos in Cosmology and Short-Baseline Oscillation Experiments, J. High Energy Phys. 11 (2013) 211.

[17] M. Archidiacono, et al., Light sterile neutrinos after BICEP-2, J. Cosmol. Astropart. Phys. 1406 (2014) 031.

[18] M. Archidiacono, et al., Pseudoscalar - sterile neutrino interactions: reconciling the cosmos with neutrino oscillations, J. Cosmol. Astropart. Phys. 1608 (2016) 067.

[19] A. Mirizzi, et al., The strongest bounds on active-sterile neutrino mixing after Planck data, Physics Letters B 726 (2013) 8–14.

[20] A. Melchiorri, et al., Sterile neutrinos in light of recent cosmological and oscillation data: a multi-flavor scheme approach, J. Cosmol. Astropart. Phys. 1 (2009) 036.

[21] A. Mirizzi, et al., Light sterile neutrino production in the early universe with dynamical neutrino asymmetries, Phys. Rev. D 86 (2012) 053009.

[22] P. A. R. Ade, et al., Planck 2013 results. I. Overview of products and scientific results, Astronomy and Astrophysics 571 (2014) A1.

[23] P. A. R. Ade, et al., Planck 2015 results. XIII. Cosmological parameters, Astronomy & Astrophysics (2015).

[24] C. Dvorkin, et al., Neutrinos help reconcile Planck measurements with both the early and local Universe, Phys. Rev. D 90 (2014) 083503.

[25] N. MacCrann, et al., Cosmic discordance: are Planck CMB and CFHTLenS weak lensing measurements out of tune?, MNRAS 451 (2015) 2877–2888.

[26] A. B. Mantz, et al., Weighing the giants - IV. Cosmology and neutrino mass, MNRAS 446 (2015) 2205–2225.

[27] R. A. Battye, A. Moss, Evidence for massive neutrinos from cosmic microwave background and lensing observations., Phys. Rev. Lett 112 (2014) 051303.

[28] Q.-G. Huang, K. Wang, S. Wang, Constraints on the neutrino mass and mass hierarchy from cosmological observations, arXiv:1512.05899 (2015).

[29] A. J. Cuesta, V. Niro, L. Verde, Neutrino mass limits: robust information from the power spectrum of galaxy surveys, Phys. Dark Univ. 13 (2015) 17.

[30] N. Palanque-Delabrouille, et al., Neutrino masses and cosmology with Lyman-alpha forest power spectrum, JCAP 1511 (2015) 11.

[31] E. Di Valentino, et al., Cosmological limits on neutrino unknowns versus low redshift priors, Phys. Rev. D 93 (2015) 083527.

[32] N. Aghanim, et al., Planck 2015 results. XI. CMB power spectra, likelihoods, and robustness of parameters, arxiv:1507.02704 (2015).

[33] A. Lewis, A. Challinor, A. Lasenby, Efficient Computation of CMB anisotropies in closed FRW models, Astrophys. J. 538 (2000) 473.

[34] J. Zuntz, et al., CosmoSIS: modular cosmological parameter estimation, Astron. Comput. 12 (2015) 45.

[35] M. Archidiacono, et al., Cosmic dark radiation and neutrinos, Adv. High Energy Phys. 2013 (2013) 191047.

[36] S. Gariazzo, et al., Light sterile neutrinos, J. Phys. G43 (2016) 033001.

[37] J. Lesgourgues, S. Pastor, Neutrino cosmology and Planck, New J. Phys. 16 (2014) 065002.

[38] S. Dodelson, L. M. Widrow, Sterile Neutrinos as Dark Matter, Phys. Rev. Lett. 72 (1994) 17.

[39] D. G. Michael, et al., The magnetized steel and scintillator calorimeters of the MINOS experiment, Nucl. Instrum. and Meth. A 596 (2008) 190–228.

[40] J. Huang, Sterile Neutrino Searches in MINOS/MINOS+ Experiment, PhD Thesis, FERMILAB-THESIS-2015-6 (2015) We use data from Figure 8.3.

[41] F. Halzen, S. R. Klein, Invited review article: IceCube: An instrument for neutrino astronomy, Review of Scientific Instruments 81 (2010) 081101.

[42] L. Wolfenstein, Neutrino oscillations in matter, Phys. Rev. D 17 (1978) 2369.

[43] S. P. Mikheev, A. Y. Smirnov, Resonant amplification of neutrino oscillations in matter and spectroscopy of solar neutrinos, Sov. J. Nucl. Phys. 42 (1985) 913.

[44] M. G. Aartsen, et al., Searches for Sterile Neutrinos with the IceCube Detector, Phys. Rev. Lett. 117 (2016) 071801.

[45] B. J. Jones, Sterile Neutrinos in Cold Climates, PhD Thesis, FERMILAB-THESIS-2015-17 (2015) We use data from Figure 3.4.10.

[46] M. Antonello, et al., A Proposal for a Three Detector Short-Baseline Neutrino Oscillation Program in the Fermilab Booster Neutrino Beam, arxiv:1503.01520 (2015).

[47] P. Huber, et al., New features in the simulation of neutrino oscillation experiments with GLoBES 3.0. (General Long Baseline Experiment Simulator), Comp. Phys. Comm. 177 (2007) 432.

[48] C. Andreopoulos, et al., The GENIE Neutrino Monte Carlo Generator, Nucl. Instrum. Meth. A614 (2010) 87–104.

[49] D. E. Groom, N. V. Mokhov, S. I. Striganov, Muon stopping power and range tables 10 mev100 tev, Atomic Data and Nuclear Data Tables 78 (2001) 183 – 356.

[50] S. Hannestad, R. S. Hansen, T. Tram, Can active-sterile neutrino oscillations lead to chaotic behavior of the cosmological lepton asymmetry?, J. Cosmol. Astropart. Phys. 2013 (2013) 032–032.

[51] K. Enqvist, K. Kainulainen, M. Thomson, Stringent cosmological bounds on inert neutrino mixing, Nucl. Phys. B 373 (1992) 498–528.

[52] L. Stodolsky, Treatment of neutrino oscillations in a thermal environment, Phys. Rev. D 36 (1987) 2273–2277.